38th International Electric Vehicle Symposium and Exhibition (EVS38) Göteborg, Sweden, June 15-18, 2025

KF-Net: Data-Driven Kalman Filter for Enhanced Battery State and Health Estimation in Electric Vehicles

Farshid Naseri and Erik Schaltz

[1]*Department of Energy, Aalborg University, Aalborg, Denmark*
Email: fna@energy.aau.dk; esc@energy.aau.dk

Executive Summary

State-of-charge (SoC) and state-of-health (SoH) estimation are critical for ensuring the performance, reliability, and safety of electric vehicles (EVs). However, accurately estimating SoH remains challenging, particularly when using model-based approaches such as Kalman filters (KFs), due to the inherent complexity and variability of battery degradation processes. As batteries age, model uncertainties increase, driven by the stochastic nature of degradation mechanisms, reducing the reliability of traditional model-based estimators. To address this challenge, we propose KF-Net, a novel data-driven Kalman filter algorithm for joint state and capacity estimation, developed within the Horizon Europe project DeepBMS. In the KF-Net architecture, a priori state estimates are generated using a battery model, while a posteriori estimates are corrected using a neural network (NN). The NN is trained on historical battery data to predict optimal Kalman gains, thereby minimizing SoH estimation errors. The method is evaluated on lithium-ion cells based on nickel manganese cobalt oxide (NMC) cathode. Preliminary results show that KF-Net outperforms the extended Kalman filter (EKF) baseline, particularly in capturing SoH trends under aging.

Keywords: Batteries, Battery Management System (BMS), Electric Vehicles (EVs), Kalman Filter (KF), State-of-Health (SoH)

1 Introduction

The growth of electric vehicles (EVs) and renewable energy systems relies heavily on advancements in lithium-ion (Li-ion) batteries and battery management systems (BMSs) [1]. A core function of the BMS is to estimate the battery's state-of-charge (SoC) and state-of-health (SoH), which are essential for ensuring performance, safety, and longevity. SoC indicates the remaining usable energy, while SoH reflects the degradation level, typically measured by changes in capacity [2].

Conventional SoC estimation techniques, such as Coulomb Counting and Open-Circuit Voltage (OCV), are either prone to error accumulation or not suitable for real-time applications. This has motivated the development of more advanced estimation methods, including machine learning (ML) and model-based approaches using Kalman filters (KFs) [3]. ML methods such as neural networks and LSTMs can handle nonlinear battery behaviors but depend on extensive training data. Model-based techniques like the Extended Kalman Filter (EKF) are more data-efficient but can struggle with model mismatch, especially as the battery ages. Regarding SoH estimation, existing techniques fall into four main categories: (1) direct measurement methods, (2) indirect analysis methods, (3) model-based methods, and (4) data-driven methods [4]. Direct measurement methods involve experimental characterization techniques conducted in the laboratory to "directly" measure the reference capacity or internal impedance of the battery. These techniques may follow standardized procedures such as those outlined in IEC62660, involving controlled capacity and resistance tests. In some cases, destructive techniques such as X-ray diffraction and scanning electron microscopy (SEM) are employed to physically characterize internal cell structure. These methods provide highly accurate SoH benchmarks, but they are not suitable for EV applications due to their offline nature and the need for cell disassembly. Indirect analysis methods estimate SoH by quantifying

degradation indicators through observable responses, using techniques such as Incremental Capacity Analysis (ICA), Differential Voltage Analysis (DVA), or ultrasonic inspection. ICA and DVA analyze the voltage-capacity curve, converting flat voltage plateaus into distinctive IC and DV peaks [3]. These peaks represent different unique shapes, amplitudes, and positions along the degradation paths, which offer great insight for SoH estimation through mixing them with ML-based methods for pattern recognition, e.g. support vector regression or Convolutional Neural Network (CNN) [5]. However, these methods face practical limitations in onboard EV applications. Specifically, accurate IC/DV curves require low charging rates (C/3 or lower), which are rarely feasible in real-world EV use [3]. Likewise, these methods rely on numerical differentiation, which increases the computational load on the BS microcontroller and amplifies measurement noise [3]. Model-based approaches typically use physics-informed aging models to predict capacity fade and internal resistance increase due to degradation mechanisms such as solid electrolyte interphase (SEI) growth or loss of lithium. These models may be derived from first principles or empirically or semi-empirically fitted to experimental data relating the battery SoH to operational parameters such as number of cycles, temperature, depth-of-discharge (DoD), and SoC. The SoH estimation RMSE level attainable with model-based approaches reported in the literature varies between 1% to 7% [3]. However, the complexity of these models often hinders their application in real-time systems [5]. Data-driven methods attempt to learn a mapping between SoH and observable battery parameters using historical battery data or based on features extracted from raw measurements. ML algorithms such as NNs and ensemble models have shown great potential to capture complex, nonlinear aging behaviors without the need for explicit modeling of physical degradation mechanisms. The disadvantage of the data-driven estimation methods is that they do not incorporate the domain knowledge, such as the state-space model (SSM) in the EKF, and consequently, they require many trainable parameters and large battery datasets [6]. However, collecting battery datasets is costly and time-consuming due to the large number of cells required for tests and the involvement of advanced and expensive test facilities. Besides this, the generalization of data-driven methods across battery chemistries and usage conditions remains an ongoing challenge.

In summary, model-based methods like EKF offer low data requirements and good estimation performance but may become computationally burdensome when complex battery models are used. While simpler models seem to be more computationally efficient, they may lack the fidelity needed to account for degradation-induced uncertainties. On the other hand, data-driven methods excel at capturing such uncertainties through learning but are constrained by data availability and training costs. Therefore, data-efficient hybrid approaches that combine the strengths of both paradigms are increasingly attractive. In this paper, we propose a hybrid estimation algorithm called KalmanNet, which integrates the robustness and structure of Kalman filtering with the adaptability of neural networks. KalmanNet leverages both model knowledge and training data to co-estimate SoC and SoH concurrently, offering a practical balance between accuracy, complexity, and data efficiency, a critical aspect that remains a challenge in the existing literature. This paper builds upon the authors' conference publication in which KalmanNet was first introduced for battery state estimation. However, in that paper, only the SoC estimation was estimated, and model uncertainties were introduced synthetically rather than using actual battery data. This work extends the conference paper by enabling the co-estimation of SoC and SoH, along with more extensive validations considering an experimental battery aging dataset.

The rest of the paper is organized as follows: In Section 2, cell specifications and explanations of the experimental work related to cell testing, test conditions, and procedures are presented. Section 3 describes the proposed KalmanNet for SoC/SoH co-estimation. Experimental results and discussions are provided in Section 4. Finally, in Section 5, the conclusions are provided.

2 Description of the experimental procedures

To collect data required for training, validation, and testing of the KalmanNet-based SoC-SoH co-estimation algorithm, automotive-grade Li-ion cells based on NMC cathode and graphite anode are tested. The cell has a nominal voltage of 3.7 V and a rated capacity of 73 A.h. Detailed specifications of the tested cells are provided in Table 1.

TABLE 1: SPECIFICATIONS OF THE TESTED LI-ION CELLS

Parameter	Value
Nominal voltage	3.7V
Rated capacity	73 A.h.
Upper voltage limit	4.2V
Lower voltage limit	2.75V
Material composition	NMC-graphite
Cell format	Pouch

A test bench based on Digatron MCT-RE (20 channels, 250 A) battery cycler and thermal chambers was used to charge-discharge cells under controlled test conditions. The schematic of the test bench is shown in Fig. 1.

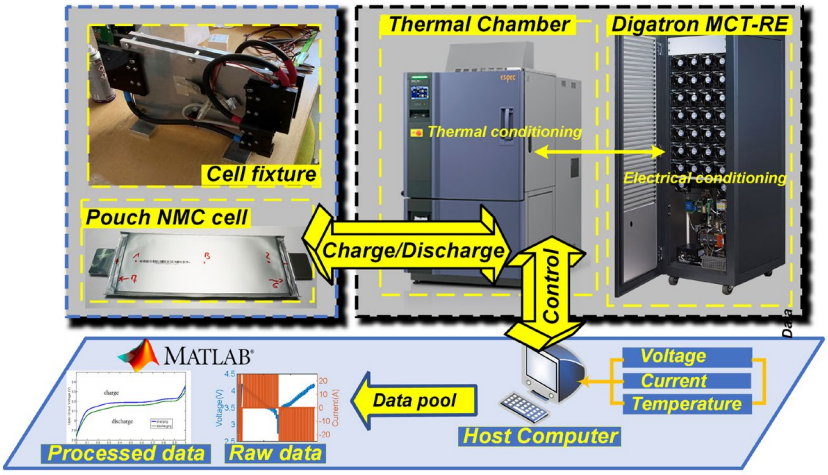

Figure 1: Schematic of the test setup used for cell testing

Different experiments involving both calendaric and cyclic aging tests at different rates, temperatures, etc. were carried out. The cyclic aging profile consisted of charge cycles based on a constant-current constant-voltage (CC-CV) protocol followed by discharge cycles at fixed rates and predefined levels of depth-of-discharge (DoD). Cells were fully characterized before and in intervals during the aging tests using reference performance tests (RPTs). The RPTs include capacity test, hybrid pulse power characteristics (HPPC) test, open-circuit voltage characteristics test (to procure the OCV-SoC relationships), and dynamic driving cycle tests. The dynamic test cycles were based on a customized driving cycle representing driving in Aarhus, Denmark (the Aarhus Driving Cycle or ADC). For the dynamic tests, the cells were initially charged to 100% SoC, then discharged according to the drive cycle profile, and subsequently recharged using the CC-CV protocol to bring the cells back to the reference test point. All tests were repeated under three temperature conditions (5°C, 25°C, and 40°C) to evaluate temperature-dependent behavior. Figure 2 shows typical RPT results at 25℃. Based on the RPT, the OCV-SoC relationships of the cells are obtained, and typical OCV-SoC curves at 25℃ are plotted in Fig. 3. The OCV-SoC curves are separately obtained during the charging and discharging processes. As seen, the charge and discharge OCV curves are similar, indicating that the level of hysteresis is negligible. Thus, to simplify the modeling process, the average of the charge and discharge curves is considered for the representation of OCV-SoC curves. The dataset created by testing different cells is used for training, testing, and validating the proposed SoC-SoH co-estimation framework based on KalmanNet.

3 Principles of the proposed KalmanNet battery state estimator

In this section, we first present and derive the original model-based EKF algorithm for real-time battery SoC-SoH estimation, which is the foundation for the KalmanNet derivation and will later be used as a

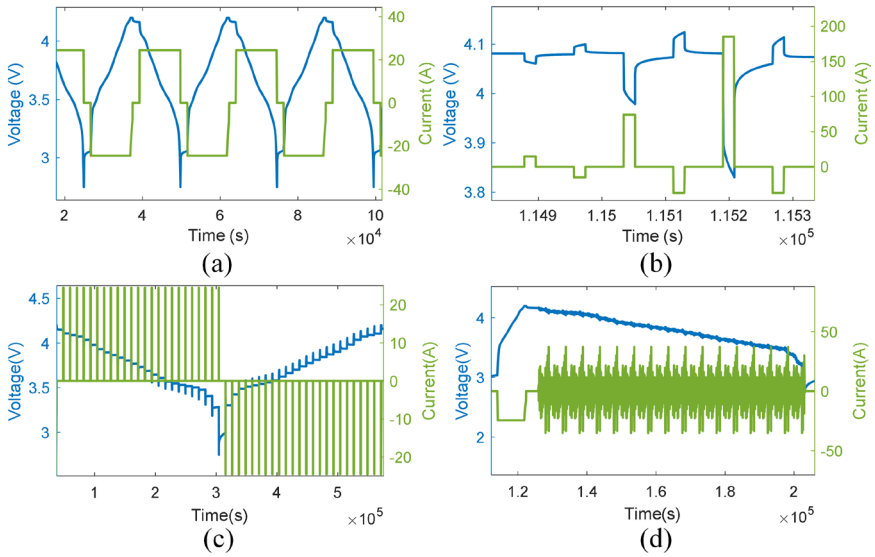

Figure 2. Typical current and voltage profiles during different RPTs at 25°C at Beginning-of-Life (BoL) (a) Capacity test (b) HPPC test (c) OCV test (d) Driving cycle test (ADC)

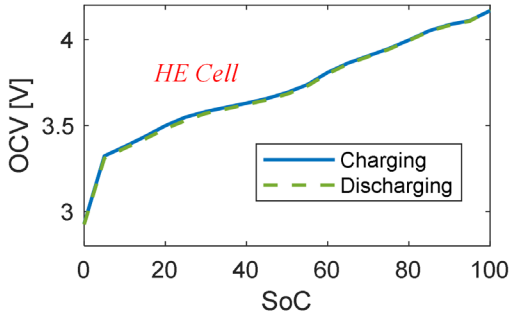

Figure 3. OCV-SoC characteristics curves at 25℃ at BoL

performance benchmark. Then, we detail the proposed co-estimation algorithm, including the KalmanNet architecture, feature extraction and definition, and training process, each discussed in separate subsections.

3.1. The model-based EKF SoC-SoH estimator

The EKF algorithm is developed here based on the formulations proposed in [7]. The implementation is fulfilled in the discrete domain, as required for final digital implementation. We assume that the battery corresponding measurement equation can be represented by the following SSM:

$$X_k = f_{k-1}\left(X_{k-1}, U_{k-1}, \omega_{k-1}\right), \quad \omega_k \sim \left(0, Q_k\right) \tag{1}$$

$$y_k = h_k\left(X_k, \upsilon_k\right), \quad \upsilon_k \sim \left(0, R_k\right), \quad y_k \in \mathbb{R}^n \tag{2}$$

where k is the sample index and U, y, and X denote the battery input, output, and state vector, respectively, while $f(\cdot)$ and $h(\cdot)$ are nonlinear functions representing the state and measurement equations. Likewise, ω and υ denote the process and measurement noises considered to have zero mean with covariances Q and R, respectively. The EKF is a recursive algorithm, which means the state vector and the matrix of estimation error covariance should be initialized:

$$\hat{X}_0^+ = E\left[X_0\right] \tag{3}$$

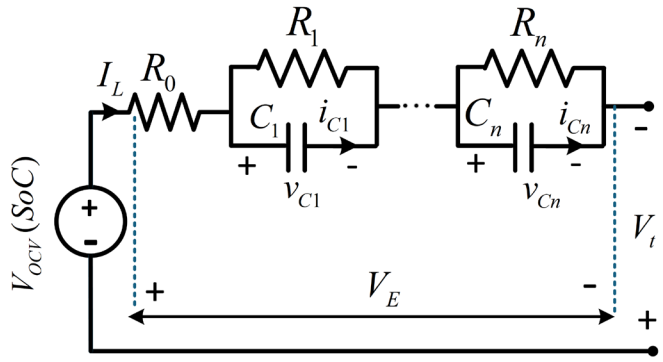

Figure 4. Second-order battery ECM used to establish the SSM

$$P_0^+ = E\left[\left(X_0 - \hat{X}_0^+\right)\left(X_0 - \hat{X}_0^+\right)^T\right] \tag{4}$$

The EKF obtains the state estimates using a two-step process: the time-update phase using the battery SSM, and the measurement-update phase using the measurement equation. The original Kalman algorithm uses a linear SSM, and to accommodate the nonlinearity, the EKF linearizes the SSM using the first-order approximation of Taylor's series expansion through the partial derivative matrices F and L as follows:

$$F_{k-1} = \left.\frac{\partial f_{k-1}}{\partial X}\right|_{\hat{X}_{k-1}^+}, \quad L = \left.\frac{\partial f_{k-1}}{\partial \omega}\right|_{\hat{X}_{k-1}^+} \tag{5}$$

The time-update of the battery state estimates $\hat{X}_k^-$ and the estimation error covariance P_k^- can be obtained as follows:

$$P_k^- = F_{k-1}P_{k-1}^+F_{k-1}^T + L_{k-1}Q_{k-1}L_{k-1}^T \tag{6}$$

$$\hat{X}_k^- = f_{k-1}\left(\hat{X}_{k-1}^+, U_{k-1}, 0\right) \tag{7}$$

For the measurement-update phase, the first-order linearization of the output can be carried out through the following derivative matrices:

$$H_k = \left.\frac{\partial h_k}{\partial X}\right|_{\hat{X}_k^-}, \quad M_k = \left.\frac{\partial h_k}{\partial \upsilon}\right|_{\hat{X}_k^-} \tag{8}$$

For obtaining the a posteriori state estimates, the measurement-update phase can ultimately be performed through the following equations:

$$K_k = P_k^- H_k^T\left(H_k P_k^- H_k^T + M_k R_k M_k^T\right)^{-1} \tag{9}$$

$$\hat{X}_k^+ = \hat{X}_k^- + K_k\left[y_k - h_k\left(\hat{X}_k^-, 0\right)\right] \tag{10}$$

$$P_k^+ = \left(I - K_k H_k\right)P_k^- \tag{11}$$

The battery SSM of (1)-(2) can be established considering the dynamic model of the battery, e.g. herein through a second-order ECM. The ECM and EKF are a widely used combination for battery state

estimation. The considered ECM is shown in Fig. 4, where I_L denotes the battery current, V_{OCV} denotes the OCV voltage, and V_t denotes the battery terminal voltage. Current is assumed to have a positive sign during discharging and a negative sign during charging. The first state equation can be derived from the Coulomb equation as follows:

$$SoC_k = SoC_{k-1} - \frac{\eta T_s I_{L,k}}{3600 C_{k-1}} \tag{12}$$

where C refers to the cell capacity, η refers to the Coulombic (charge) efficiency, and T_s is the sampling time. To obtain other state equations, we consider that the dynamic part of the ECM containing the ohmic resistor and the two resistive-capacitive networks, can be represented through the second-order transfer function in (13), where cross-multiplication yields (14):

$$\frac{V_{E,k}}{I_{L,k}} = \frac{b_0 + b_1 z^{-1} + b_2 z^{-2}}{1 + a_1 z^{-1} + a_2 z^{-2}} \tag{13}$$

$$V_{E,k} = -a_1 V_{E,k-1} - a_2 V_{E,k-2} + b_0 I_{L,k} + b_1 I_{L,k-1} + b_2 I_{L,k-2} \tag{14}$$

where z^{-1} is the discrete unit delay function. Another battery dynamic state is the cell's capacity *C*, which gradually reduces over time due to battery degradation. We are particularly interested in estimating the cell capacity, as it represents the battery SoH. Considering that the changes in *C* are small and gradual within the estimation time steps T_s, one can approximate $C_k \approx C_{k-1}$ leading to the following equation:

$$C_k = C_{k-1} + \omega_4 \tag{15}$$

where ω_4 denotes a random noise. We will introduce this state equation to the overall battery SSM and co-estimate it alongside the cell's SoC. Co-estimating SoC and SoH allows the estimator to better capture the underlying coupled dynamics and inherent correlations between the states. By defining $x_{1,k} = SoC_k$, $x_{2,k} = V_{E,k}$, $x_{3,k} = V_{E,k-1}$, $x_{4,k} = C_k$, and $U_k = [u_{1,k} \quad u_{2,k} \quad u_{3,k}] = [I_{L,k} \quad I_{L,k-1} \quad I_{L,k-2}]$, the state equations can be derived from (12)-(15) as follows:

$$x_{1,k} = x_{1,k-1} - \frac{\eta T_s u_{1,k}}{3600 x_{4,k-1}} + \omega_1 \tag{16}$$

$$x_{2,k} = -a_1 x_{2,k-1} - a_2 x_{3,k-1} + b_0 u_{1,k} + b_1 u_{2,k} + b_2 u_{3,k} + \omega_2 \tag{17}$$

$$x_{3,k} = x_{2,k-1} + \omega_3 \tag{18}$$

$$x_{4,k} = x_{4,k-1} + \omega_4 \tag{19}$$

where ω_1 to ω_4 are the process noise with characteristics defined in (1). The process noise accounts for the uncertainty in the process model and states, and is considered to be an additive term here. The output equation can be derived by applying KVL to the circuit model of Fig. 4:

$$V_{t,k} = V_{OCV,k}(S0C) + V_{E,k} \Rightarrow y_k = V_{OCV,k}(SoC) + x_{2,k} + \upsilon \tag{20}$$

where υ is the measurement noise as in (2) and $V_{OCV,k}$ is a nonlinear function of the SoC and temperature and is established using the OCV-SoC characteristic tests in Section 2. The OCV model can be implemented by fitting OCV-SoC data to an appropriate regressor function, such as a polynomial function, or alternatively using two-dimensional look-up tables. In this paper, polynomial functions of appropriate orders are used to represent the OCV models for the NMC cells. The last state variable is defined based on

the cell terminal voltage as $x_{5,k} = V_{t,k}$. Since the cell's terminal voltage $V_{t,k}$ is a measurable variable, this definition will ensure the system's observability. The state equation can be obtained using the derivation of (20), which leads to the following:

$$\begin{aligned} V_{t,k} &= V_{t,k-1} + \left.\frac{\partial V_{OCV,k}(SoC)}{\partial SoC}\right|_{SoC_{k-1}} .\left(SoC_k - SoC_{k-1}\right) + V_{E,k} - V_{E,k-1} \\ \Rightarrow x_{5,k} &= x_{5,k-1} + \left.\frac{\partial V_{OCV,k}(x_1)}{\partial x_1}\right|_{x_{1,k-1}} .\left(x_{1,k} - x_{1,k-1}\right) + x_{2,k} - x_{3,k} + \omega_5 \end{aligned} \tag{21}$$

Equations (16) to (21) represent the state and output equations corresponding to $f(\cdot)$ and $h(\cdot)$ in (1) and (2), respectively. Finally, the battery states x_1 to x_5 can be co-estimated using the EKF algorithm with equations (3) to (11), in a sample-by-sample manner. The partial derivative matrices *F*, *L*, *H*, and *M* can be in part pre-calculated from the state equations derived before. Accordingly, one can write *M*=1 and $L \in \mathbb{R}^{5\times5}$ is a unity matrix of size 5, while *F* and *H* can be obtained as follows:

$$F_{k-1} = \left.\frac{\partial f_{k-1}}{\partial X}\right|_{\hat{X}^+_{k-1}} = \begin{bmatrix} 1 & 0 & 0 & \frac{\partial f_1}{\partial x_4} & 0 \\ 0 & -a_1 & -a_2 & 0 & 0 \\ 0 & 1 & 0 & 0 & 0 \\ 0 & 0 & 0 & 1 & 0 \\ \frac{\partial V_{OCV}}{\partial x_1} & 1 & -1 & 0 & 1 \end{bmatrix} \quad H = \begin{bmatrix} \frac{\partial V_{OCV}}{\partial x_1} \\ 1 \\ -1 \\ 0 \\ 1 \end{bmatrix}^T \tag{22}$$

As seen in (22), only a few entries need to be computed in real-time, while the remaining entries are fixed, which simplifies the embedded implementation. In practice, it is expected that the battery SSM parameters ($a_1, a_2, b_0, b_1,$ and b_2) will change under different operating conditions of temperature and SoC, as well as due to the battery aging process. Thus, the model parameters should also be estimated and updated in real-time to maintain the accuracy of the EKF algorithm. The architectural block diagram of the EKF-based SoC/SoH estimator is shown in Fig. 5.

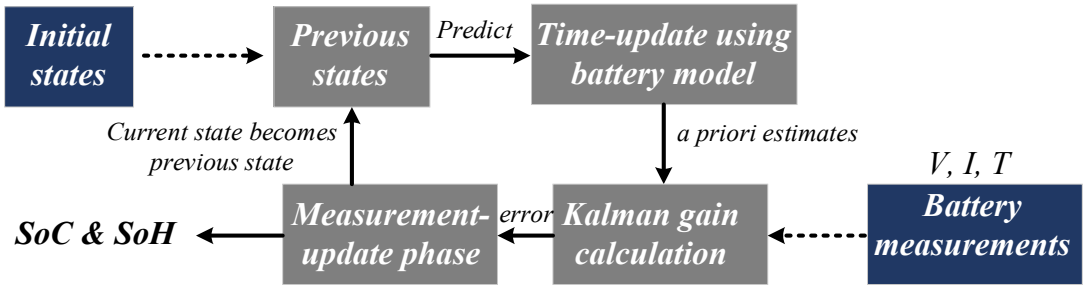

Figure 5. Block diagram of the EKF-based state estimation

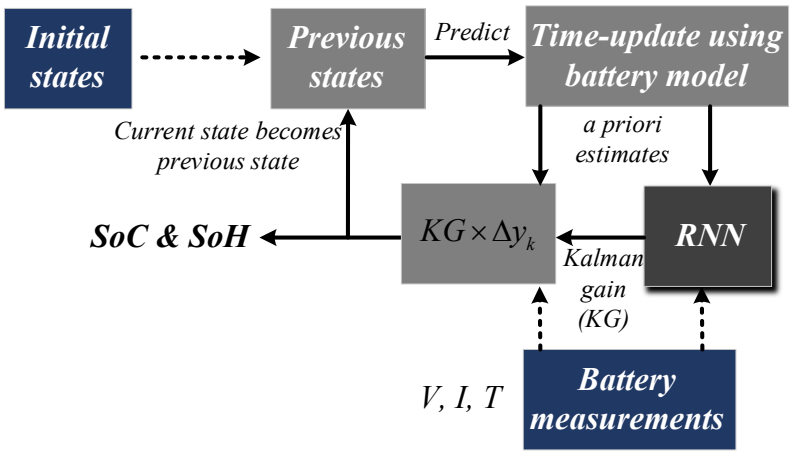

(b)

Figure 6. Block diagram of the EKF-based state estimation

KalmanNet combines the EKF-based state estimator with a recurrent neural network (RNN) to tackle the modeling uncertainties and nonlinearities arising from cell aging. In the EKF-based state estimator, the covariances R and Q are normally not known and must be selected by trial and error, which are used in the KF process to obtain the Kalman gain based on (9). Here, the KalmanNet learns the Kalman gain statistics directly from data and integrates it into the overall Kalman filter process flow [8]-[10]. The time-update phase of the KalmanNet is merely based on (7), while the measurement-update phase is fulfilled using the innovation term $\Delta y_k = y_k - h_k(\hat{X}_k^-, 0)$. Contrary to the EKF, the Kalman gain is not calculated explicitly using (9); rather, it is obtained by training an RNN using battery data. The internal memory of RNN allows it to capture and track the underlying noise dynamics. The block diagram of KalmanNet is depicted in Fig. 6. The input features are designed as follows:

$$\Delta y_k = \hat{y}_k - y_k \tag{23}$$

$$\Delta \hat{X}_k^- = \hat{X}_{k-1}^- - \hat{X}_{k-1}^+ \tag{24}$$

The output of the RNN contains the vector of Kalman gains $K \in \mathbb{R}^{5\times 1}$. The architecture of the RNN includes two fully connected layers (FCLs) as input and output, and a gate recurrent unit (GRU) in between them. The activation function type is considered to be rectified linear unit (ReLU) in the middle part of the network and a tangent hyperbolic (tanh) before the output layer. The training of the RNN is performed in a supervised end-to-end manner using the back propagation technique and stochastic gradient descent algorithm, and considering the following loss function:

$$LF = \left\| X_k - \hat{X}_k^+ \right\| \tag{25}$$

4 Results and discussions

The KalmanNet SoC-SoH estimator is trained and tested using the MATLAB/SIMULINK environment. The dynamic ADC tests at different stages of battery life are used to train the KalmanNet, while the RPTs are used for parameterization of the EKF and the battery model in (1) and (2).

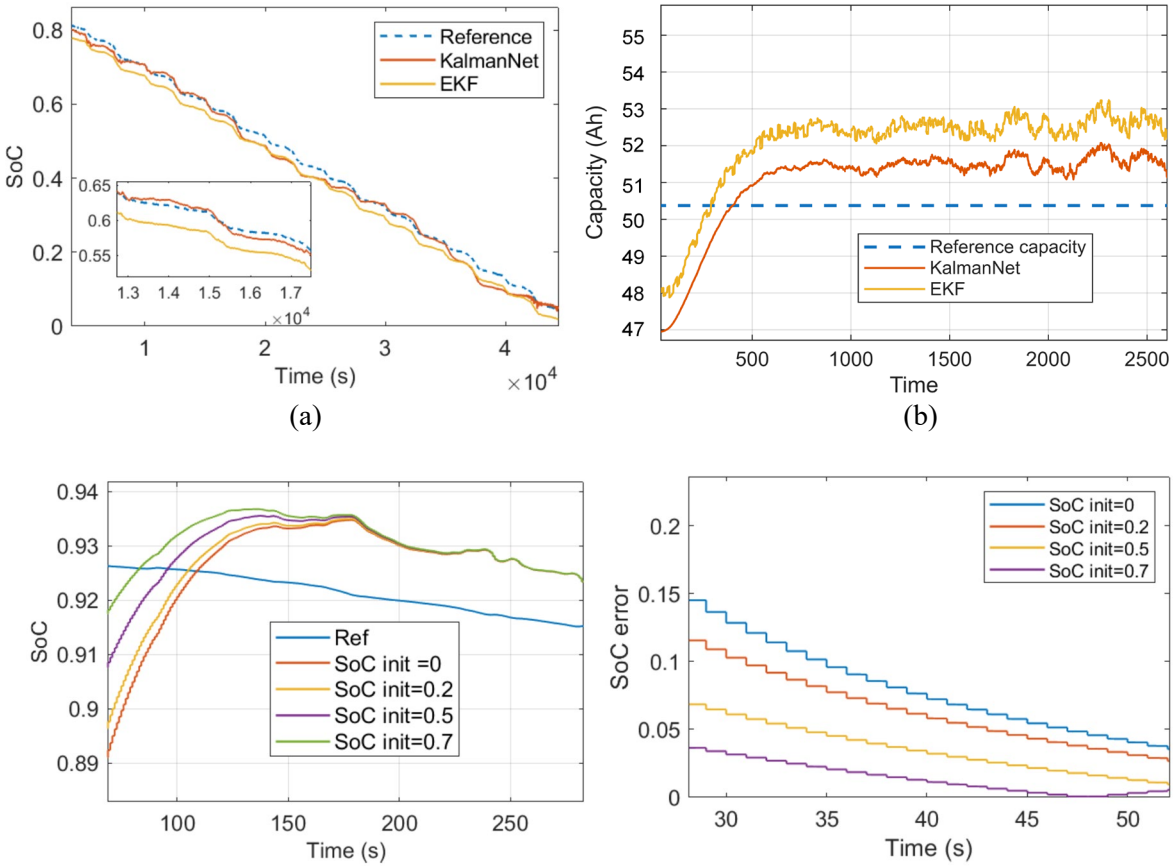

Figure 7. Simulation results of EKF and KalmanNet (a) SoC estimation over one ADC cycle at 25 °C (b) Capacity (SoH) estimation over a dynamic cycle for aged cells (c) SoC estimation considering different initial SoC values in algorithms (d) SoC estimation error for different initialization settings

Fig. 7 presents the SoC and SoH estimation results over a dynamic ADC cycle at 25 °C, comparing the performance of the EKF and KalmanNet algorithms. To ensure a fair comparison, the covariance matrices in the EKF are selected to achieve the best possible estimation accuracy. In Fig. 7(a), the SoC estimation results demonstrate that while both methods can accurately track the SoC, KalmanNet outperforms EKF due to its superior ability to handle model uncertainties. The capacity estimation results in Fig. 7(b) support a similar conclusion for SoH, highlighting KalmanNet's improved accuracy in estimating the capacity of aged cells. To assess filter convergence, various initialization conditions were tested. The results show that, regardless of the initial SoC value, KalmanNet consistently converges to the ground truth in the early stages of the simulation. A summary of the state estimation performance across different test scenarios is provided in Table 2.

TABLE 2. SUMMARY OF THE STATE ESTIMATION RESULTS USING EKF AND KALMANNET

		5 degC	25 degC	40 degC
EKF	SoC	0.028	0.025	0.019
	SoH	0.052	0.049	0.046
KalmanNet	SoC	0.015	0.012	0.011
	SoH	0.031	0.029	0.026

In the table, simulation results at different temperature conditions for an aged cell (SoH ≈ 70%) are listed, showing that KalmanNet consistently achieves lower estimation errors for both SoC and SoH across all temperatures, demonstrating its robustness and superior performance compared to EKF, particularly under varying thermal conditions.

5 Conclusions and future work

This paper presents KalmanNet, a data-driven Kalman filter framework for the joint estimation of battery SoC and SoH. Built upon the model-based EKF, KalmanNet replaces the traditional computation of Kalman gains with a RNN that learns gain statistics directly from historical battery data. This hybrid approach enhances robustness against model inaccuracies and nonlinearities, particularly those arising from battery aging and temperature-dependent behavior. A second-order ECM was employed to describe the battery dynamics, with both SoC and capacity (as a proxy for SoH) included in the state vector. The algorithm was trained and validated using real experimental data from NMC-based lithium-ion cells subjected to dynamic driving profiles and aging conditions at multiple temperatures. Simulation results demonstrated that KalmanNet consistently outperforms the EKF in terms of estimation accuracy, convergence speed, and robustness, especially under aging and varying thermal conditions.

Future work will focus on several directions. First, we aim to optimize the KalmanNet architecture (e.g., layer size, depth, and activation functions) to improve estimation accuracy while reducing computational complexity. Second, we will investigate real-time deployment of KalmanNet on embedded platforms typical of battery management systems, with attention to memory and processing constraints. Additionally, we plan to extend the methodology to handle online learning and adaptation, enabling the network to update itself incrementally during operation as new data becomes available. Lastly, we will explore the generalization of KalmanNet across different cell chemistries and usage patterns to assess its applicability in a wider range of EV and energy storage systems.

Acknowledgments

The paper is prepared within the framework of the European project DeepBMS funded by the European Union's Horizon Europe Program under Marie Skłodowska-Curie Actions with grant agreement No. 101064083. The authors also acknowledge the EU project HELIOS funded by the European Union's Horizon 2020 research and innovation programme under grant agreement No. 963646.

References

[1] F. Naseri, E. Schaltz, D.-I. Stroe, A. Gismero, and E. Farjah, "An enhanced equivalent circuit model with real-time parameter identification for battery state-of-charge estimation," IEEE Transactions on Industrial Electronics, vol. 69, no. 4, pp. 3743-3751, 2021.

[2] F. Naseri et al., "Digital twin of electric vehicle battery systems: Comprehensive review of the use cases, requirements, and platforms," Renewable and Sustainable Energy Reviews, vol. 179, p. 113280, 2023.

[3] O. Demirci, S. Taskin, E. Schaltz, and B. A. Demirci, "Review of battery state estimation methods for electric vehicles-Part II: SOH estimation," *Journal of Energy Storage*, 96, p.112703, 2024

[4] O. Demirci, S. Taskin, E. Schaltz, and B. A. Demirci, "Review of battery state estimation methods for electric vehicles-Part I: SOC estimation," *Journal of energy storage*, 87, p.111435, 2024

[5] D. Roman, S. Saxena, V. Robu, M. Pecht, and D. Flynn, "Machine learning pipeline for battery state-of-health estimation," *Nature Machine Intelligence*, 3(5), pp.447-456, 2021.

[6] X. Sui, S. He, S. B. Vilsen, J. Meng, R. Teodorescu, and D. I. Stroe, "A review of non-probabilistic machine learning-based state of health estimation techniques for Lithium-ion battery," *Applied Energy*, 300, p.117346, 2021.

[7] D. Simon, 2006. "Optimal state estimation: Kalman, H infinity, and nonlinear approaches," John Wiley & Sons.

[8] G. Revach, N. Shlezinger, X. Ni, A. L. Escoriza, R. J. Van Sloun, and Y. C. Eldar, "KalmanNet: Neural network aided Kalman filtering for partially known dynamics," *IEEE Transactions on Signal Processing*, 70, pp.1532-1547, 2022.

[9] X. Ni, G. Revach, and N. Shlezinger, "Adaptive KalmanNet: Data-driven Kalman filter with fast adaptation," In ICASSP 2024-2024 *IEEE International Conference on Acoustics, Speech*

and Signal Processing (ICASSP) (pp. 5970-5974). IEEE, 2024

[10] G. Revach, N. Shlezinger, R. J. Van Sloun, and Y. C. Eldar, "Kalmannet: Data-driven kalman filtering," In ICASSP 2021-2021 *IEEE International Conference on Acoustics, Speech and Signal Processing (ICASSP)* (pp. 3905-3909). IEEE, 2021.

Presenter Biography

Farshid Naseri is a Ph.D. expert in vehicular and storage technologies, currently serving as a Marie-Curie postdoctoral fellow at Aalborg University (AAU Energy), Denmark. He received his Ph.D. and M.Sc. in Electrical Power Engineering in 2019 and 2015 and his B.Sc. degree in Control Engineering in 2013. He has contributed to different EU projects related to the development of battery systems with TRL levels from 2 to 8 including HELIOS, DeepBMS, HEROES, and iBattMan. His research interests encompass electric vehicles, battery systems, control systems, and power electronic systems design. Dr. Naseri is an active member of the IEEE Young Professionals and a board member of the *Vehicle Engineering Section* in Machines.